Maximizing the Photocatalytic Activity of Metal-Organic Frameworks with Aminated-Functionalized Linkers: Sub-stoichiometric Effects in MIL-125-NH2

Matthew B. Chambers, Xia Wang, Laura Ellezam, Ovidiu Ersen, Marc Fontecave, Clément Sanchez, Laurence Rozes, Caroline Mellot-Draznieks

Maximizing the Photocatalytic Activity of Metal-Organic Frameworks with Aminated-Functionalized Linkers: Sub-stoichiometric effects in MIL-125-NH2

Matthew B. Chambers,†,‡,# Xia Wang,†,# Laura Ellezam,†,§ Ovidiu Ersen, ‖ Marc Fontecave, †,# Clément Sanchez, §,# Laurence Rozes *,§ and Caroline Mellot-Draznieks*†,#

† Laboratoire de Chimie des Processus Biologiques, UMR 8229 CNRS, UPMC Univ Paris 06, Collège de France, 11 Marcelin Berthelot, 75231 Paris Cedex 05, France

§ Sorbonne Universités, UPMC Univ Paris 06, CNRS, Collège de France, Laboratoire de Chimie de la Matière Condensée de Paris, 4 Place Jussieu, 75252 Cedex 05, France

‖ Institut de Physique et Chimie des Matériaux de Strasbourg (IPCMS), UMR 7504 CNRS-Université de Strasbourg (UdS), 23 rue du Loess, 67037 Strasbourg Cedex 08, France

Institut de Chimie du Collège de France, Collège de France, 11 Marcelin Berthelot, 75231 Paris Cedex 05, France

ABSTRACT: Despite the promise of utilizing metal-organic frameworks (MOFs) as highly tunable photocatalytic materials, systematic studies that interrogate the relationship between their catalytic performances and the amount of functionalized linkers are lacking. Aminated linkers are known to enhance the absorption of light and afford photocatalysis with MOFs under visible-light irradiation. However, the manner in which the photocatalytic performances are impacted by the amount of such linkers is poorly understood. Here, we assess the photocatalytic activity of MIL-125, a TiO_2/1,4-benzenedicarboxylate (bdc) MOF for the oxidation of benzyl alcohol to benzaldehyde when increasing amounts of bdc-NH_2 linkers (0%, 20%, 46%, 70% and 100%) are incorporated in the framework. Analytical TEM allowed assessing the homogeneous localization of bdc-NH_2 in these mixed-linker MOFs. Steady state reaction rates reveal two regimes of catalytic performances: a first *linear* regime up to ~50% bdc-NH_2 into the hybrid framework whereby increased amounts of bdc-NH_2 yielded increased photocatalytic rates, followed by a *plateau* up to 100% bdc-NH_2. This unexpected "saturation" of the catalytic activity above ~50% bdc-NH_2 content in the framework whatever the wavelength filters used, demonstrates that amination of all linkers of the MOF is not required to obtain the maximum photocatalytic activity. This is rationalized on the basis of mixed-valence Ti^{3+}/Ti^{4+} intermediate catalytic centers revealed by Electron Spin Resonance measurements and recent knowledge of lifetime excited states in MIL-125-type of solids.

INTRODUCTION

Harnessing the energy of light to trigger chemical reactions typically requires semiconducting photocatalytic metal oxide materials, with titanium dioxide (TiO2) remaining one of the most widely studied.[1] Recently, metal-organic frameworks (MOFs), a class of crystalline structures composed of organic and inorganic building blocks are attracting growing interest as alternative photocatalysts. One remarkable advantage of MOFs over other porous solids lies in their versatile and modular frameworks, whereby they may be synthesized from many different organic linkers and functionalized with a variety of chemical species.[2] In addition, because of their tunable optical properties[3] MOFs have rapidly emerged as valuable platforms in key areas such as optoelectronics,[4] light harvesting and photo-induced heterogeneous catalysis.[5] There are thus abundant reports of MOFs that possess photocatalytic activities and take advantage of their synthetic and post-synthetic versatility in order to catalyze organic transformations,[6] proton reduction,[7] CO_2 reduction,[8] or water oxidation,[9] amongst other reactions.

As a subfield of research, the modulation of MOFs' optical response was extensively explored and is now well rationalized with respect to the role of the metal centers and the linkers in terms of length and substituents.[10] In contrast to semiconductors,[11] systematic studies that interrogate the relationship between the catalytic performances and the amount of functionalized linkers (i.e. considered as sub-stoichiometric dopants) are very scarce.[12] Comparisons between functionalized MOFs are binary: the functionalized linker is either entirely present (100 molar %) or absent. Shen *et al.*[12a] studied the electronic effect of bdc-X (X = H, NH_2, NO_2, Br) in UiO-66 on the photocatalytic activities in water treatment and found they are linearly correlated with the Hammett coefficients of the linker's substituent. The combination of multiple linkers functionalized with electron-donating (bdc-NH_2) and withdrawing substituents (bdc-X, X= H, F, Cl, Br) in

UiO-66 has been reported by Maligal-Ganesh *et al.* as a promising route to enhance catalytic performances for the oxidation of alcohols.[12b] However, little attention has been given overall to identify optimal linkers compositions. The scarcity of such studies stems from the notorious challenge of characterizing mixed-linker MOFs.[2b,13] Since severe limitations in their characterization by diffraction are imposed by the positional disorder of similar linkers within the framework, sophisticated techniques are required to assess the apportionment of multiple linkers and differentiate between a homogeneous distribution or segregated nanodomains.[14] These include NMR techniques,[15] photothermal induced resonance,[16] or microspectrophotometry.[17] The non-destructive characterization of mixed-linker MOFs is thus far from routine and remains a critical issue if we want to rationalize their catalytic properties.[18]

In this multifaceted context, the report in 2009 of MIL-125[19] $Ti_8O_8(OH)_4(bdc)_6$ (Figure 1) as a photocatalyst under UV irradiation was a breakthrough and triggered intense efforts towards the synthesis of new Ti-based MOFs.[20] Yet, one-pot synthesis of new ones remains scarce, resulting in MIL-125 and derivatives standing as the most illustrative examples of their potential uses in photocatalysis.[21] These span a large range of reactions, such as the oxidation of alcohols into aldehydes,[22] of amines into imines, the oxidative desulfurization of dibenzothiophene,[24] and the reduction of CO_2,[25] protons,[26] or Cr(VI).[27]

MIL-125 absorbs light in the UV region with a photochromic behavior due to the Ti^{IV}/Ti^{III} photoactive redox centers. Using bdc-NH_2 in place of bdc allows the synthesis of the isostructural MIL-125-NH_2 and a shift of light absorption towards the visible region,[25,28] providing an efficient strategy to convert bdc-based MOFs into visible-light harvesters.[29] The ligand-metal-charge transfer (LMCT) and the separation of electrons and holes (on Ti-oxo clusters and –NH_2 groups, respectively) upon photoexcitation were clearly established by EPR, flash photolysis and theory.[30] The role of –NH_2 groups in promoting long-lived photo-excited states was recently show using transient spectroscopies.[31] While it is now established that bdc-NH_2 linkers greatly affect the optical response of MIL-125,[28b] the question of their quantitative impact on the catalytic performances remains however unanswered.

Herein, we investigate at various wavelengths the photocatalytic performances of a series of mixed-linker MIL-125s synthesized with various amounts of bdc and bdc-NH_2 linkers, denoted MIL-125-NH_2-%. Analytical TEM experiments in the 2D chemical energy filtered TEM (EFTEM) mode[32] provide evidence at the nanoscale for the homogeneous distribution of bdc-NH_2 within the MOFs crystallites. The photocatalytic oxidation of benzyl alcohol (Scheme 1) is then used as an initial show case reaction to evaluate the performances of this series of solids as a function of the amination level of the MOF. Unlike inorganic doped solids, we find that the photocatalytic activity of MIL-125-NH_2-% solids is not strictly *linearly* correlated to the bdc-NH_2 content. We rather show that maximum catalytic activity is reached at a recurrent sub-stoichiometric composition in bdc-NH_2 linkers whatever the wavelength regime used and propose a rationale for this unexpected behavior.

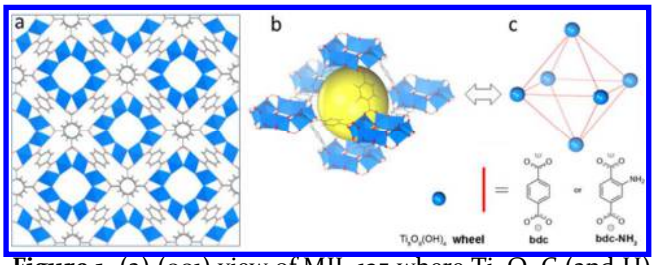

Figure 1. (a) (001) view of MIL-125 where Ti, O, C (and H) are in blue, red and grey, respectively; (b) Octahedral cage in MIL-125; a yellow sphere materializes the accessible volume; (c) Octahedral cage where Ti_8-wheels formed of edge/corner-sharing TiO_8 octahedra are depicted as blue spheres and linkers as red struts.

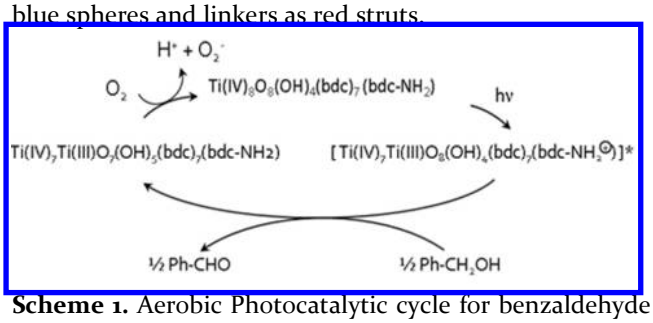

Scheme 1. Aerobic Photocatalytic cycle for benzaldehyde production in MIL-125-NH_2-%. One bdc is replaced in the chemical formula with one bdc-NH_2 linker in order to illustrate the stabilization of the hole on the –NH_2 group[31] upon illumination coupled with the formation of one Ti^{3+}-Ti^{4+} mixed valence pair evidenced in this work.

RESULTS AND DISCUSSION

The series of mixed-linker MIL-125-NH_2-% solids were synthesized under hydrothermal conditions by varying the ratio of bdc : bdc-NH_2 acids in their synthetic mixtures, namely MIL-125, MIL-125-NH_2-20%, -46%, -70% and -100% where % refers to the proportion of bdc-NH_2 linkers determined from ^{13}C NMR (Figure S1). X-Ray powder diffraction patterns and scanning electron microscopy images correspond well to those already reported and confirmed that all aminated solids possess high crystallinity and are isostructural to the parent MIL-125 solid (Figure S2).[19] N_2-physisorption analysis revealed expected porosities, with BET surface areas in the [893-1024 m^2/g] range for the MIL-125-NH_2-20%, -46%, and -100% solids and a distinctly higher value for the -70% one (1300 m^2/g). All aminated MOFs demonstrated a similar absorption onset (ca 475 nm) in their UV-visible absorption spectra, i.e. a red shifted optical band gap of ~2.6 eV compared to that of MIL-125 (~3.7 eV) (Figure S3). The visible-light absorption is due to the conjugated π electron transition from the amine containing chromophores to the Ti-oxo clusters. The –NH_2 motif is responsible for this reduced optical band gap (*vs* MIL-125) as a result of an increase in the energy level of the valence band localized on the organic units whilst the energy of the conduction band localized on the Ti-based nodes remains unchanged.[28b]

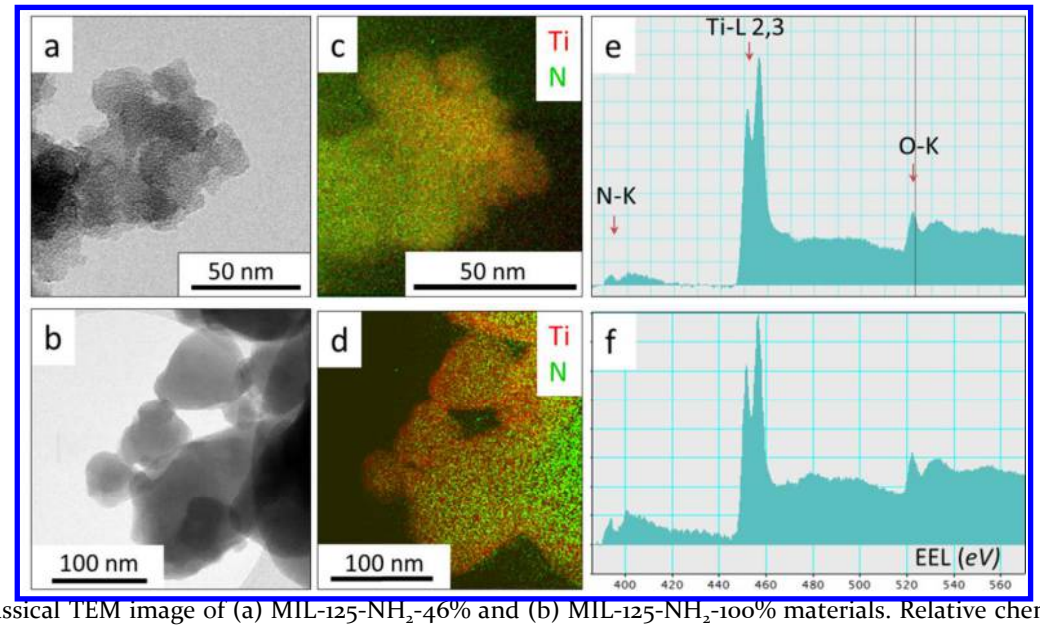

Figure 2. Classical TEM image of (a) MIL-125-NH_2-46% and (b) MIL-125-NH_2-100% materials. Relative chemical map (Ti: red, N: green) obtained from the 2D chemical EFTEM analysis of (c) MIL-125-NH_2-46% and (d) MIL-125-NH_2-100%. Both samples show a good homogeneity of the aminated species. (e) and (f) show the EELS spectra of MIL-125-NH_2-46% and MIL-125-NH_2-100% samples, respectively.

While the above characterizations reflect the effective incorporation of the aminated linkers within the MOFs, they leave unaddressed their homogenous or heterogeneous spatial distribution within the frameworks. In MIL-125-NH_2-% solids, the bdc-NH_2 linkers may be distributed over the 12 positions available for the organic linker per unit cell. There is the possibility of having segregated nanodomains or a mixture of phases. Considering that aminated linkers are the only molecules that contain nitrogen atoms, the presence of N is a handle as to their spatial distribution. A local characterization technique with chemical sensitivity and a resolution in the nm range was thus required to map the N atoms at the nanoscale.

Electron Energy Loss Spectroscopy (EELS) allowed the detection of nitrogen by spatially analyzing the inelastic electrons corresponding to its K-edge (401 eV) inside a selection of MIL-125-NH_2-% solids. TEM images on typical aggregates of superimposed plate-like grains are shown for MIL-125-NH_2-46% and -100% materials in Figures 2a and 2b, respectively. An Energy Filtered TEM (EFTEM) study allowed us to explore the microstructural features within the MIL-125-NH_2-46% and -100% specimen and to assess the distribution of the aminated linkers, which was compared with the distribution of titanium species, also mapped in EFTEM using the Ti $L_{2,3}$ edge (456 eV). This chemical analysis revealed that both Ti and N (in red and green, respectively, in Figure 2) are uniformly distributed in both MIL-125-NH_2-46% (Figure 2c) and -100% (Figure 2d) samples at the nanoscale. Moreover, when comparing both solids, the N: Ti ratio was found to vary from 0.13 to 0.3 in line with the ratio used in their synthetic mixtures. Importantly, evidence is provided here that MIL-125-NH_2-% types of solids possess a homogenous and random repartition of the bdc-NH_2 linkers within the crystallites, which allows us excluding the formation of segregated nanodomains comprising either bdc or bdc-NH_2, and the mixture of aminated and non-aminated crystalline phases.

Figure 3 shows the photocatalytic performances of MIL-125-NH_2-% assessed for the selective oxidation of benzyl alcohol to benzaldehyde at various wavelengths, 325, 415, 450 and 490 nm. Blank experiments without illumination or catalyst did not yield any quantifiable amounts of benzaldehyde after 8 hours of reaction. Also, no photocatalytic activity was observed when a 490 nm long pass filter was used. All solids were active under the other regimes (i.e. λ>325, λ>415, λ>450 nm) as displayed in Figure 3. The formation of benzaldehyde in the course of the reaction was quantified by ^{1}H NMR as illustrated in Figure S5.

Photocatalytic assays revealed an unexpected and recurrent behavior, whereby the catalytic formation of benzaldehyde occurs within two distinct regimes. At low incorporation levels of bdc-NH_2 (0 to ~50%), catalytic rates were found to increase in a linear fashion with the % bdc-NH_2 amounts, for example reaching a reaching a rate of photocatalysis of 275 nmol hr^{-1} mg^{-1} for MIL-125-NH_2-46% when a 325 nm long pass filter was used (Figure 3a). Surprisingly, at levels greater than 50% of bdc-NH_2, a stationary regime or *plateau* is observed where no further increase in aldehyde production turnover frequency is noted, i.e. MIL-125-NH_2-46%, -70% and -100% catalysts having similar activities. The first linear regime follows the general intuition that as more bdc-NH_2 linkers are incorporated into the framework, the MOF is expected to absorb light more efficiently, and thus catalysis is likewise faster. This is in line with many previous reports that correlate the enhanced photocatalytic activities of aminated MOFs to their improved optical absorption properties when compared to their non aminated counterparts.[6d,22,25,29a]

The *plateau* in the ~50-100% bdc-NH_2 range, i.e the absence of increase in the photocatalytic activity when more

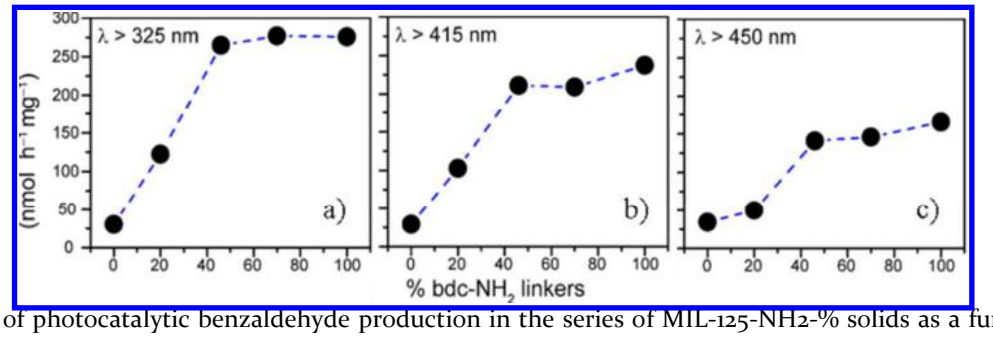

Figure 3. Rates of photocatalytic benzaldehyde production in the series of MIL-125-NH2-% solids as a function of the % bdc-NH_2 content. Three long pass filters were used: (a) 325 nm, (b) 415 nm and (c) 450 nm. No product was detected within 8 h with a 490 nm long pass filter. The percent standard deviation for the measurements is inferior to 10% (see SI, pp 6).

bdc-NH_2 linkers are incorporated into the MOF, is indeed counter-intuitive. We initially considered it could result from limitations in either substrate or product diffusion through the pores of the materials. However, the lack of an induction period to the detection of benzaldehyde indicates no limitation in product diffusion (see Figure S4). Benzyl alcohol diffusion into the material was ruled out as the y-intercept of the kinetic traces of benzaldehyde evolution are close to the value of trace benzaldehyde initially present in the benzyl alcohol solvent (Figure S4). Limitation of O_2 diffusion is also unlikely as oxygen deficient photolysis with these solids would result in an observable dark green color in the otherwise white or yellow materials assigned to a build-up of Ti^{3+} states in the inorganic nodes. This was not observed ruling out a lack of O_2. Additionally, the observed catalytic rates were independent of whether or not the sample mixture was re-aerated during the course of photolysis, further suggesting that availability of O_2 was not limiting.

Interestingly, the same *plateau* behavior in photocatalysis rates was found whatever the pass filter used, i.e. 325, 415 or 450 nm (Figures 3a-b-c, respectively). However, the oxidation rate at the *plateau* decreased when switching from 325 to 415 and to 450 nm long pass filters. If experimental factors such as diffusion of substrates were limiting the activity, photocatalysis rates would be expected to maximize at the same diffusion limited values. However, this is not the case as distinct maximum photocatalysis rates are found for different ranges of light energy used. Finally, in light of the characterizations of the samples (see SI), we may exclude that such important differences of catalytic performances between the samples have their origin in their different crystallinity, morphology, porosity or apportionment of the linkers, the latter being shown to be random. The enhanced porosity of the MIL-125-NH_2-70% solid when compared to that of the -46% one (with 412 m^2/g additional porosity) should result in enhanced catalytic activity. However, in view of their similar catalytic activities, we may conclude that porosity differences are indeed not responsible for variations in their photocatalytic activity over the various light regimes.

Overall, the *plateau* beyond the 50% bdc-NH_2 composition level reflects the intrinsic photocatalytic activity of the solids. It appears most likely that an optimal tuning of catalytic properties of MIL-125-NH_2-% lies at 50% bdc-NH_2. The recurrence of the *plateau* regardless of the range of light used for irradiation thus opens the question of its origin.

Our results above show that the non-aminated bdc linkers do not participate to the photocatalytic events when illuminated in the visible or UV (see the marginal activities of the MIL-125 sample Figures 3a-b-c). Amino groups boost the photocatalytic performances of the MIL-125-NH_2-% solids in line with the recent evidence that -NH_2 groups act as hole stabilizers and prolong the life time of the excited states in MIL-125-NH_2-100%.[30b,31] In the present work, the linear correlation we observe between catalytic rates and bdc-NH_2% in the [0-50%] composition range directly reflects the incremental beneficial impact of the aminated linkers on the MIL-125-NH_2-% solids' catalytic performances. Still, the recurring *plateau* in the photocatalytic activities in the [~50-100%] bdc-NH_2 composition range reveals that additional productive catalytic centers are not further generated when more bdc-NH_2, *i.e.* above ~50%, are introduced into the framework.

A closer look at the crystal structure of the MIL-125-type hybrid framework suggests that such limitations may emanate from its unique connectivity made of corner- and edge-sharing titanium octahedra forming Ti_8-wheels connected to each other through the organic linkers (Figure 1). The photon-dependent formation of a reduced Ti^{3+} catalytic center occurs upon electron transfer from one bdc-NH_2 linker to one Ti^{4+} center[30b,31] may lead to a photoinduced mixed valent state, *i.e.* a Ti^{3+}-Ti^{4+} pair, within the Ti_8-wheel. This wheel-structure could impose electrostatic penalties as more such Ti^{3+}-Ti^{4+} pairs are formed photochemically, thus limiting the participation of additional bdc-NH_2 linkers to the generation of productive catalytic centers in MIL-125-NH_2-% solids. Even with 100% aminated linkers after complete formation of mixed valent states (half of the Ti have been reduced) further reduction of Ti^{4+} may become unfavorable.

To shed more light on the nature of catalytically active centers, electron spin resonance spectroscopy (ESR) experiments were carried out at different temperatures on the MIL-125-NH_2-100% impregnated with benzylic alcohol (see experimental). While the non-irradiated MIL-125-NH_2-100% powders were ESR silent, after UV irradiation,

a strong axial ESR signal appeared at 77K. The magnetic parameters exhibit the characteristic values of paramagnetic Ti^{3+} centers in a distorted rhombic oxygen ligand field ($g_\perp$ = 1.924, $g_\parallel$ = 1.890).[33] (See Figure S6). A small anisotropic signal close to free electron g values corresponding to paramagnetic O_2^- species (g ≈2.00) is also observed.

When the temperature is increased, the signal corresponding to paramagnetic O_2^- species is still present at room temperature. On the contrary, the Ti^{3+} ESR signal broadens and practically disappears when ESR spectra is recorded at RT (see Figure S6). This linewidth broadening of the Ti^{3+} resonance can be associated to an increase of the electron hopping frequency with temperature. This behavior is characteristic of thermally activated electron hopping in mixed valence metal-oxo clusters.[34] In the present study the observed features correspond to electron hopping from Ti^{3+} to Ti^{4+} sites ($3d^1$ to $3d^0$ configurations).

As previously analyzed for transition metal-oxo based solids, a line broadening in the range 77K-300K corresponds to activation energies of about 0.05 eV. [34,35] Such mixed valence compounds correspond to class II following the classification proposed by Robin and Day.[36] Upon UV irradiation, MIL-125-NH_2-100% exhibits a photodarkening associated as reported to a broad band located in the near infrared region which is the characteristic feature of an optically activated electronic transfer between Ti^{3+} and Ti^{4+} centers.[19,36] Clearly, the dark coloration observed here with MIL-125-NH_2-100% presents a weaker contrast when compared with the strong dark blue colorations that we observed for photoirradiated MIL-125[19] and titanium oxo-PHEMA nanocomposites.[36b]

This weaker stability of the reduced Ti^{3+} state (shorter life time of the reduced fundamental state) for MIL-125-NH_2-100% can be related to a faster oxidative fading for MIL-125-NH_2-100% when compared to that of MIL-125. The shorter life time of the reduced fundamental state and the longer life time of the excited state as determined by femtosecond transient absorption spectroscopy[30,31] are likely responsible for the superior catalytic activity of MIL-125-NH_2-%.

Finally, evidence is provided here that the mixed valence bimetallic centers or Ti^{3+}-O-Ti^{4+} pairs act as the catalytic centers responsible in MIL-125-NH_2% solids for the transformation of alcohols in carbonylated compounds, thus supporting the observation that only 50% of aminated linkers are required to reach the maximum catalytic activity.

CONCLUSION

In summary, we have evaluated the photocatalytic performances of the Ti-based MIL-125 synthesized with increasing amounts of aminated linkers, bdc-NH_2 vs bdc (0, 20, 46, 70, 100%). The characterization of the apportionment of the bdc-NH_2 linkers in these mixed-linker solids unambiguously reveals their homogenous thus random distribution within the frameworks. The photocatalytic activity of this series of MOFs towards the oxidation of benzyl alcohol was monitored in situ via ^{1}H NMR with several different long pass filters. Interestingly, the experimental rates of reactions reveal that a *plateau* in catalytic activities is reached around 50% bdc-NH_2 content. This *plateau* is attributed to the intrinsic catalytic performance of the hybrid solids as opposed to factors such as substrate/product diffusion, changes in structure, variation in porosity or homogeneity of the samples. A substoichiometric number of the aminated linkers indeed contribute to the catalysis. The present work thus reveals that the amination of all linkers in the MOF (i.e. 100% bdc-NH_2) is not required to obtain a maximum photocatalytic activity, although the use of aminated linkers is associated with improved optical absorption, as shown by a linear regime in the [0-50%] bdc-NH_2range. The maximum photocatalytic activity at ~50% bdc-NH_2 content is to be correlated to the occurrence of the mixed valence Ti^{4+}-Ti^{3+} state within the Ti_8-wheels in MIL-125's crystal structure. Finally, the work broadly highlights the importance in considering the optimal functionalized linkers composition in MOFs when targeting enhanced photocatalytic performances, especially as it may be structure-dependent and thus vary from one MOF to another. We believe that these results provide important insight into general conditions wherein sub-stoichiometric linker exchanges or post-synthetic functionalization can afford efficient light absorption while also stimulating further investigations towards the role of sub-stoichiometric linker exchanges in tuning photocatalytic activity within MOFs.

EXPERIMENTAL SECTION

Synthesis and Characterizations. A series of mixed-linker MIL-125-NH_2-% were synthesized with increasing amounts of bdc-NH_2 linkers within the hybrid framework. The compounds were prepared according to the previously reported solvothermal self-assembly procedures.[28a] In short the series of mixed-linker MIL-125-NH_2-% compounds were prepared by replacing part of the bdc acid molecules with bdc-NH_2 acid molecules in the synthetic mixtures, containing 0, 20, 46, 70 and 100% of bdc-NH_2 linker as determined from ^{13}C NMR measurements. The synthesized solids are named MIL-125-NH_2-% where % refers to the amount of aminated linker of the hybrid solids as estimated from NMR characterizations. Powder diffraction patterns were obtained from a Bruker D8 instrument. SEM snapshots were acquired from a Hitachi S-3400N microscope. UV data were collected on a Cary 5000 instrument. Nitrogen physisorption measurements were performed on a Belsorp max instrument.

NMR Methods. Synthesized mixed-linker MIL-125 solids were characterized by ^{13}C solid state Nuclear Magnetic Resonance (NMR) experiments. Quantitative conditions were applied in order to determine the experimental contents of bdc and bdc-NH_2 linkers in the mixed ligand solids MIL-125-NH_2-%. NMR experiments were undergone on a 7 T Bruker Avance III spectrometer corresponding to 75 MHz for ^{13}C. 7 mm zirconia rotors were spun at 5 kHz in a standard dual resonance broadband probe. In order to suppress ^{13}C probe signal, zgbs sequence was used (θ-180°-180°) with θ=30° and a

relaxation delay of 30 s. This delay has been checked to provide full relaxation to get quantitative results. Additionally, 50 kHz 1H SPINAL-64 decoupling[34] was applied during acquisition but not during relaxation. Spectra were modelled using dmfit program.[35]

TEM Analyses. TEM and EFTEM analyses were performed on a JEOL 2100F transmission electron microscope equipped with a post-column GATAN Tridiem energy filter. The samples were crushed, dispersed in ethanol and put on an ultrasonic bath during 5 min. The K and Ti maps were determined by EFTEM using the three windows method applied to the energy filtered images recorded at both N-K edge (401 eV) and Ti L2,3 edge (456 eV). For each element, three energy filtered images were acquired in the EFTEM mode, the two first recorded by selecting two energy windows (energy width of 20 eV) before the ionization edge and the last one by selecting a 20 eV energy window after the ionization edge, allowing thus proper background subtraction and calculation of the chemical maps.

Catalytic Assays. Photocatalytic assays were performed using a 300W Xe Arc lamp at room temperature with various wavelength filters. A typical sample included between 4-5 mg of a MIL-125-NH_2-% material transferred into a 1 cm quartz cuvette with a Pyrex extension at the top to provide a larger gaseous headspace for the sample. To the cuvette, 4 ml of neat benzyl alcohol were charged via syringe and a Teflon stir bar was added. The cuvette was then sealed with a septum under ambient air and thoroughly wrapped with parafilm in order to minimize evaporative losses. The prepared sample in the cuvette was placed in front of the light in front of a magnetic stir plat and aliquots were periodically removed for analysis. Every second hour during the first 8 hours aliquots (0.3 ml) were removed and immediately added to 0.3 ml of an NMR solvent with an internal standard (CD_3CN/ 1 mM Toluene). One aliquot was assayed after 24 hours reaction confirming the stability of the material. Assays were performed while using four different long pass filters: 325, 415, 450 and 490 nm. Analyses of benzaldehyde production were performed using a 300 MHz Bruker NMR. The area of the benzaldehyde resonance (10.2 ppm) could be integrated and compared to the toluene standard to afford facile determination of product yield. Changes in sample volumes caused by aliquot removal were carefully considered. The concentration of benzaldehyde throughout a kinetic assay was calculated using the volume of the sample at the time of aliquot removal. The volume at any given measurement was taken to be the initial volume minus the product of 0.3 ml and the number of aliquots removed preceding the measurement of interest.

ESR Methods. ESR spectra of irradiated MIL-125-NH_2-100% impregnated with benzyl alcohol have been recorded at room temperature and 77K on a band X (9.3 GHz) JEOL FA-300 spectrophotometer with a microwave power of 2 mW and a magnetic field modulation amplitude of 100 KHz.

ASSOCIATED CONTENT

Supporting Information

The Supporting Information is available free of charge on the ACS Publications website. Synthesis and characterization details, NMR, microscopy methods, catalytic assays (PDF).

AUTHOR INFORMATION

Corresponding Authors

laurence.rozes@upmc.fr

caroline.mellot-draznieks@college-de-france.fr

Present Addresses

‡ Department of Chemistry, University of North Carolina at Chapel Hill, Chapel Hill, North Carolina 27599-3290, United States.

ACKNOWLEDGMENT

Drs. G. Laurent from LCMCP and F. Averseng from the Laboratoire de Réactivité de Surface are acknowledged for ^{13}C solid state NMR and ESR experiments, respectively. The authors also thank Dr. N. Elgrishi for assistance in the design of experimental protocols for the photocatalysis assays, data analysis of MIL-125 derivatives that were instrumental in the development of our understanding of the photocatalysis results. We acknowledge support from Fondation de l'Orangerie for individual Philanthropy and its donors.

REFERENCES

(1) Schneider, J.; Matsuoka, M.; Takeuchi, M.; Zhang, J. L.; Horiuchi, Y.; Anpo, M.; Bahnemann, D. W. *Chem. Rev.* **2014**, *111*, 9919.
(2) (a) Cohen S.M. *Chem. Rev.* **2012**, *112*, 970. (b) Cohen S. M. *J. Amer. Chem. Soc.* **2017**, *139*, 2855. (b) Deng, H. X., Doonan, C. J.; Furukawa, H.; Ferreira, R.B.; Towne, J.; Knobler, C. B.; Wang B.; Yaghi, O. M. *Science* **2010**, *327*, 846.
(3) (a) Alvaro, M.; Carbonell, E.; Ferrer, B.; Llabrés i Xamena, F. X.; García, H. *Chem. Eur. J.* **2007**, *13*, 5106. (b) Silva, C. G.; Corma, A. L.; García, H. *J. Mater. Chem.* **2010**, *20*, 3141.
(4) Stavila, V.; Talin, A. A.; Allendorf, M. D. *Chem. Soc. Rev.* **2014**, *43*, 5994.
(5) (a) Wang, C.; Xie, Z.; deKrafft, K. E.; Lin, W. *J. Am. Chem. Soc.* **2011**, *133*, 13445. (b) Nasalevich, M. A.; van der Veen, M.; Kaptejin, F.; Gascon, J. *CrystEngComm.* **2014**, *16*, 4919. (c) Wang, J. L.; Wang, C.; Lin, W. *ACS Catal.* **2012**, 2, 2630. (d) Horiuchi, Y.; Toyao, T.; Takeuchi, M.; Mastuoka, M.; Anpo, M. *Phys. Chem. Chem. Phys.* **2013**, *15*, 13243. (e) Zhang, T.; Lin, W. *Chem. Soc. Rev.* **2014**, *43*, 5982. (f) Foster, M. E.; Azoulay, J. D.; Wong, B. M.; Allendorf, M. D. *Chem. Sci.* **2014**, 5, 2081.
(6) (a) Wang, C.-C.; Li, J. R.; Lv, X.-L.; Zhang, Y.-Q.; Guo, G. *Energy Environ. Sci.* **2014**, *7*, 2831. (b) Long, J.; Wang, S.; Ding, Z.; Wang, S.; Zhou, Y.; Huang, L.; Wang, X. *Chem. Commun.* **2012**, *48*, 11656. (c) Wu, P.; He, C.; Wang, J.; Peng, X.; Li, X.; An, Y.; Duan, C. *J. Am. Chem. Soc.* **2012**, *134*, 14991. (d) Laurier, K. G. M., Vermoortelle, F.; Ameloot, R.; DeVos, D. E.; Hofkens, J.; Roeffaers, M. B. J. *J. Am. Chem. Soc.* **2013**, *135*, 14488.
(7) (a) Silva, C.G.; Luz, I.; Llabres i Xamena, F. X.; Corma, A., Garcia, H. *Chem. Euro. J.* **2010**, *16*, 11133. (b) Pullen, S.; Fei, H.; Orthaber, A.; Cohen, S.; Ott, S. *J. Am. Chem. Soc.* **2013**, *45*, 16997. (c) Sasan, K.; Lin, Q.; Mao, C.; Feng, P. *Chem. Commun.* **2014**, *50*, 10390. (d) Nasalevich, M. A.; Becker R.; Ramos-Fernandez, E. V.; Castellanos, S.; Veber, S. L.; Fedin

M. V.; Kapteijn, F.; Reek J. N. H.; van der Vlugt J. I.; Gascon J. *Energy Environ. Sci.* **2015,** *8*, 364.
(8) (a) Wang, S.; Yao, W.; Lin, J.; Ding, Z.; Wang, X. *Angew. Chem. Int. Ed.*, **2014**, *53*, 1034. (b) Wang, D.; Huang, R.; Liu, W.; Sun, D.; Li, Z. *ACS Catal.* **2014**, *4*, 4254. (c) Chambers, M. B.; Wang, X.; Elgrishi, N.; Hendon, C. H.; Walsh, A.; Bonnefoy, J.; Canivet, J.; Quadrelli, E. A.; Farrusseng, D.; Mellot-Draznieks, C.; Fontecave, M. *ChemSusChem* **2015**, *8*, 603.
(9) (a) Meyer, K.; Ranocchiari, M.; van Bokhoven, J. A. *Energy Environ. Sci.* **2015**, *8*, 1923. (b) Chi, L.; Xu, Q.; Liang, X.; Wang, J.; Su, X. *Small* **2016**, *12*, 1351.
(10) (a) Fuentes-Cabrera, M.; Nicholson, D. M.; Sumpter, B. G.; Widom, M. *J. Chem. Phys.* **2005**, *123*, No. 124713. (b) Gascon, J.; Hernandez-Alonso, M. D.; Almeida, A. R.; van Klink, G. P. M.; Kapteijn, F.; Mul, G. *ChemSusChem* **2008**, *1*, 981. (c) Choi, J. H.; Choi, Y. J.; Lee, J. W.; Shin, W. H.; Kang, J. K. *Phys. Chem. Chem. Phys.* **2009**, *11*, 628. (d) Kuc, A.; Enyashin, A.; Seifert, G. *J. Phys. Chem. B* **2007**, *111*, 8179. (e) Yang, L.-M.; Ravindran, P.; Vajeeston, P.; Tilset, M. *RSC Adv.* **2012**, *2*, 1618.
(11) (a) Etacheri, V.; Di Valentin, C.; Schneider, J. ; Bahnemann, D. ; Pillai, S. C. *J. Photochem. Photobiol. C : Photochem Rev.* **2015**, *25*, 1. (b) Dozzi, M. V.; Selli, E. *J. Photochem. Photobiol. C : Photochem Rev.* **2013**, *14*, 13. (c) Liu, G.; Wang, L.; Sun, C.; Yan, X.; Wang, X.; Chen, Z.; Smith, S.C.; Cheng, H.-M.; Qing Lu, G. *Chem. Mater.* **2009**, *21*, 1266.
(12) (a) Shen, L.; Liang, R.; Luo, M.; Jing, F.; Wu, L. *Phys. Chem. Chem. Phys.* **2015**, *17*, 117. (b) Goh, T.W.; Xiao, C. X.; Maligal-Ganesh, R. V.; Lin, X. L.; Huang, W. Y.; *Chem. Eng. Sci.* **2015**, *124*, 45.
(13) Sue, A. C.-H.; Mannige, R. V.; Deng, H.; Cao, D.; Wang, C.; Gandara, F.; Stoddart, J. F.; Whitelam, S.; Yaghi, O. M. *P. N. A. S.* **2015**, *112*, 5591.
(14) (a) Cheetham, A. K.; Bennett, T. D.; Coudert, F. X.; Godwin, A. L. *Dalton Trans.* **2016**, *45*, 4113. (b) Cliffe, M. J. Wan, W. Zou, X. D. Chater, P. A. Kleppe, A. K. Tucker, M. G. Wilhelm, H. Funnell, N. P. Coudert, F. X. Goodwin, A. L. *Nat. Commun.* **2014**, *5*, 4176.
(15) (a) Kong, X.; Deng, H.; Yan, F.; Kim, J.; Swisher, J. A.; Smith, B.; Yaghi, O. M.; Reimer, J. A. *Science* **2013,** *341*, 882. (b) Krajnc, A.; Kos, T.; Logar, N. Z.; Mali, G. *Angew. Chem. Int. Ed.* **2015**, *54*, 10535. (c) Rossini, A. J.; Zagdoun, A.; Lelli, M.; Canivet, J.; Aguado, S.; Ouari, O.; Tordo, P.; Rosay, M.; Maas, W. E.; Coperet, C.; Farrusseng, D.; Emsley, L.; Lesage A. *Angew. Chem. Int. Ed.* **2012**, *51*, 123.
(16) Katzenmeyer, A. M.; Canivet, J.; Holland, G.; Farrusseng, D.; Centrone, A. *Angew. Chem. Int. Ed.* **2014**, *53*, 2852.
(17) Liu, C.; Li, T.-Y.; Feura, E. S.; Zhang, C.; Rosi, N. *J. Am. Chem. Soc.* **2015**, *137*, 10508.
(18) (a) Lescouet, T.; Kockrich, E.; Bergeret, G.; Pera-Titus, M.; Aguado, S.; Farrusseng, D. *J. Mater. Chem.* **2012**, *22*, 10287. (b) Hendon, C. H.; Bonnefoy, J.; Quadrelli, E. A.; Canivet, J.; Chambers, M. B.; Rousse, G.; Walsh, A.; Fontecave, M.; Mellot-Draznieks, C. *Chem. Eur. J.* **2016**, *22*, 3713.
(19) Dan Hardi, M.; Serre, C.; Frot, T.; Rozes, L.; Maurin, G.; Sanchez, C.; Férey, G. *J. Am. Chem. Soc.* **2009**, *131*, 10857.
(20) (a) Rozes, L.; Sanchez, C. *Chem. Soc. Rev.* **2011**, *40*, 1006. (b) Gao, J.; Miao, J.; Li, P.-Z.; Teng, W. Y.; Yang, L.; Zhao, Y.; Liu, B.; Zhang, Q. *Chem. Commun.* **2014**, *50*, 3786. (c) Zou, L.; Feng, D.; Liu, T.-Fu; Chen, Y.-P.; Yuan, S.; Wang, K.; Wang, X.; Fordham, S.; Zhou, H.-C. *Chem. Sci.* **2016**, *7*, 1063.
(21) Amador, R. N.; Carboni, M.; Meyer, D. *Mater. Lett.* **2016**, *166*, 327.
(22) Nasalevich, M. A.; Goesten, M. G.; Savenije, T. J.; Kapteijn, F.; Gascon, J. *Chem. Commun.* **2013**, *49*, 10575.
(23) Sun, D.; Ye, L.; Li, Z. *Appl. Catal. B: Environ.* **2015**, *164*, 428.
(24) Kim, S.N.; Kim, J.; Kim, H. Y. K.; Cho, H. Y.; Ahn W. S.; *Catal. Today* **2013**, *204*, 85.
(25) Fu, Y.; Sun, D.; Chen, Y.; Huang, R.; Ding, Z.; Fu, X.; Li, Z. *Angew. Chem. Int. Ed.* **2012**, *51*, 3364.
(26) (a) Horiuchi, Y.; Toyao, T.; Saito, M.; Mochizuki, K.; Iwata, M.; Higashimura, H.; Anpo, M.; Matsuoka, M. *J. Phys. Chem. C* **2012**, *116*, 20848. (b) Nasalevich, M. A.; Becker, R.; Ramos-Fernandez, E. V.; Castellanos, S.; Veber, S. L.; Fedin, M. V.; Kapteijn, F.; Reek, J. N. H.; van der Vlugt, J. I.; Gascon, J. *Energy Environ. Sci.* **2015**, *8*, 364.
(27) Wang, H.; Yuan, X.; Wu, Y.; Zeng, G.; Chen, X.; Leng, L.; Wu, Z.; Jiang, L.; Li, H. *J. Hazard. Mat.* **2015**, *286*, 187.
(28) (a) Hendon, C. H.; Tiana, D.; Fontecave, M.; Sanchez, C.; D'arras, L.; Sassoye, L. Rozes, C.; Mellot-Draznieks, C. *J. Am. Chem. Soc.* **2013**, *135*, 10942. (b) Moreira, M. A.; Santos, J. C.; Ferreira, A. F. P.; Loureiro, J. M.; Ragon, F.; Horcajada, P.; Yot, P. G.; Serre, C.; Rodrigues, A. E. *Microporous Mesoporous Mater.* **2012**, *158*, 229.
(29) (a) Sun, D. R.; Fu, Y. H.; Liu, W. J.; Ye, L.; Wang, D. K.; Yang, L.; Fu, X. Z.; Li, Z. H. *Chem. Eur. J.* **2013**, *19*, 14279. (b) Sun, D.; Liu, W.; Qiu, M.; Zhang, Y.; Li, Z.; *Chem. Commun.* **2015**, *51*, 2056. (d) Lee, Y.; Kim, S.; Kang, J. K.; Cohen, S. M. *Chem. Commun.* **2015**, *51*, 5735. (e) Shen, L.; Liang, S.; Wu, W.; Liang, R.; Wu, L. *Dalt. Trans.* **2013**, *42*, 13649.
(30) (a) de Miguel, M.; Ragon, F.; Devic, T.; Serre, C.; Horcajada, P.; García, H. *ChemPhysChem* **2012**, *13,* 3651. (b) Nasalevich, M.A. ; Hendon, C. H.; Santaclara, J. G. ; Svane, K.; van der Linden, B.; Veber, S. L.; Fedin, M. V.; Houtepen, A. J., van der Veen, M. A.; Kapteijn, F.; Walsh, A.; Gascon, J. *Scientific Reports* **2016**, *6*, 23676.
(31) Santaclara, J. G. ; Nasalevich, M.A. ; Castellanos, S. ; Evers, W. H. ; Spoor, F. C. M. ; Rock, K. ; Siebbeles, L. D. A., Kapteijn, F.; Grozema, F.; Houtepen. A.; Gascon, J.; Hunger, J.; van der Veen, M. A. *ChemSusChem.* **2016**, *9*, 388.
(32) Carenco, S; Moldovan, S., Roiban, L.; Florea, I.; Portehault, D.; Vallé, K., Belleville, P.; Boisière, C.; Rozes, L. ; Mézailles, N. ; Drillon, M. ; Sanchez, C. ; Ersen, O. *Nanoscale*, **2016**, *8*, 1260.
(33) Goodman, B.A.; J. B. Raynor. Advances in Inorganic Chemistry and Radiochemistry. Ed. H.J. Emeleus,. Sharpe, A.G Academic Press, New York and London. **1970**, *13*, 185.
(34) (a)Sanchez, C.; Livage, J.; Launay, J. P.; Fournier M.; Jeannin, Y. *J. Am. Chem. Soc.* **1982**, *104*, 3194. (b) Sanchez, C.; Livage, J.; Launay, J. P.; Fournier M., *J. Am. Chem. Soc.* **1983**, *105*, 6817.
(35) Sanchez, C.; Henry, M.; Grenet, J.C.; Livage, J. *J. Phys. C: Solid State Phys.* **1982**, *15*, 7133.
(36) (a)Robin M.B. and Day P. *Adv. Inorg. Chem. Radiochem.* **1967**, *10*, 247. (b) Kameneva, O.; Kuznestov, A. I.; Smirnova, L. A.; Rozes, L.; Sanchez, C.; Alexandrov, A.; Bityurin, N.; Chhor, K.; Kanaev, A. *J. Mater. Chem.* **2005**, *15*, 3380.
(37) Fung, B. M.; Khitrin, A. K.; Ermolaev, K. *J. Magn. Reson.* **2000**, *142*, 97.
(38) Massiot, D. ; Fayon, F. ; Capron, M. ; King, I.; Le Calve, S.; Alonso, B.; Durand, J. O.; Bujoli, B.; Gan, Z. H.; Hoatson, G. *Magn. Reson. Chem.* **2002**, *40*, 70.

TOC graphic

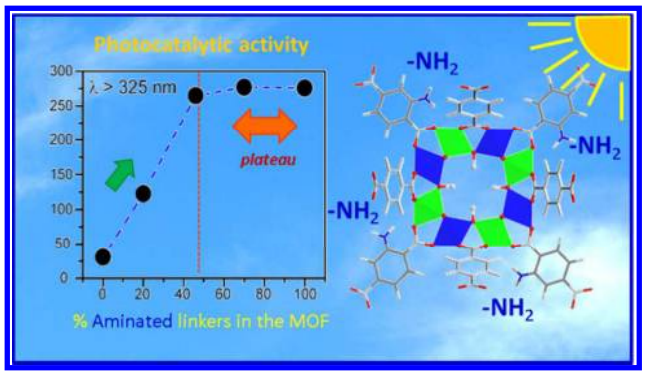
Photocatalytic activity
λ > 325 nm
plateau
300
250
200
150
100
50
0
0
20
40
60
80
100
% Aminated linkers in the MOF
-NH2
-NH2
-NH2
-NH2

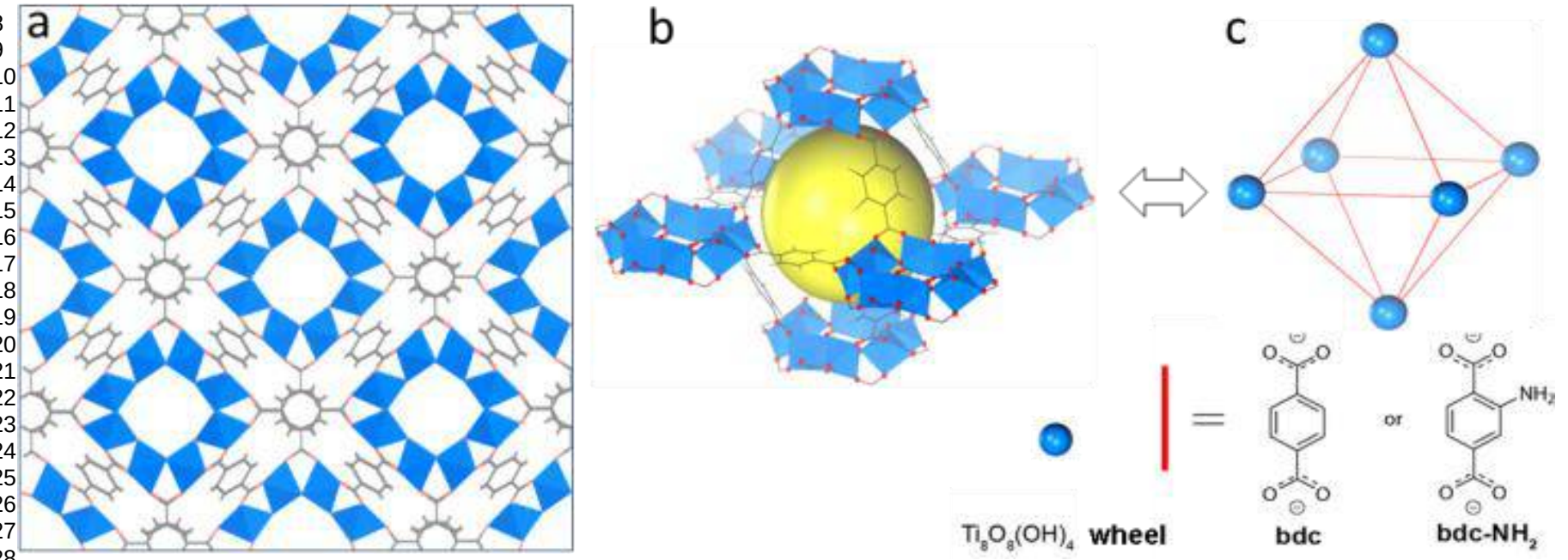
a
b
c
Ti8O8(OH)4 wheel
bdc
or
NH2
bdc-NH2

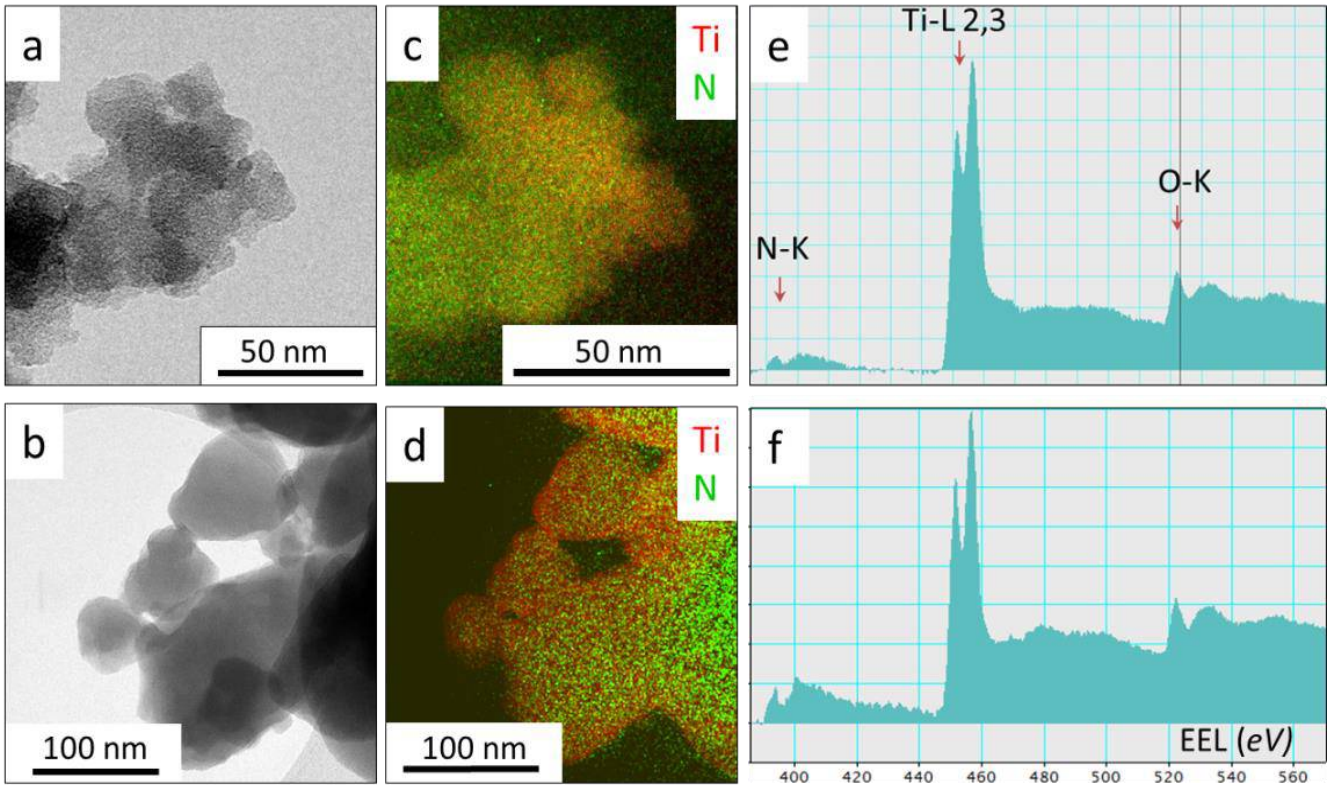
a
50 nm
c
Ti
N
50 nm
e
Ti-L 2,3
O-K
N-K
b
100 nm
d
Ti
N
100 nm
f
EEL (eV)
400
420
440
460
480
500
520
540
560

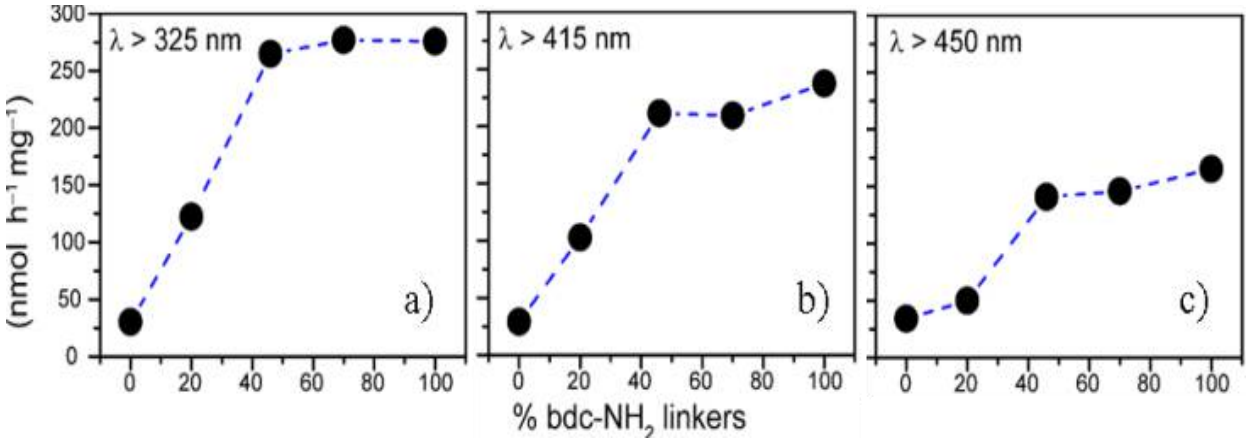
λ > 325 nm
λ > 415 nm
λ > 450 nm
a)
b)
c)
(nmol h⁻¹ mg⁻¹)
% bdc-NH2 linkers
0
50
100
150
200
250
300
0
20
40
60
80
100

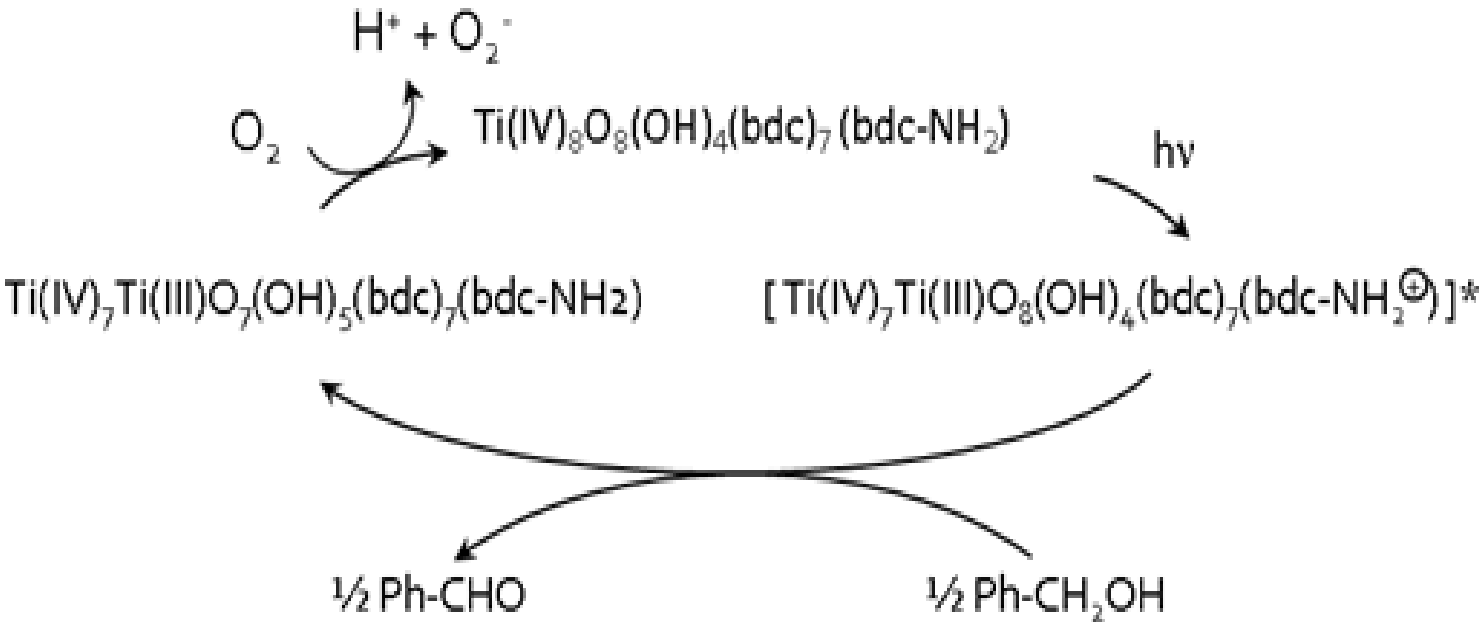
H+ + O2-
O2
Ti(IV)8O8(OH)4(bdc)7(bdc-NH2)
hv
Ti(IV)7Ti(III)O7(OH)5(bdc)7(bdc-NH2)
[Ti(IV)7Ti(III)O8(OH)4(bdc)7(bdc-NH2⊕)]*
½ Ph-CHO
½ Ph-CH2OH